Displacive phase transition at the 5/3 monolayer of Pb on Ge(001)

D. Cvetko,[1,2,3] F. Ratto,[2,4] A. Cossaro,[2] G. Bavdek,[2,3] A. Morgante,[2,5] and L. Floreano[2,*]
[1]*Department of Physics, University of Ljubljana, Ljubljana, Slovenia*
[2]*Laboratorio TASC dell'Istituto Nazionale per la Fisica della Materia, Trieste, Italy*
[3]*J. Stefan Institute, Ljubljana, Slovenia*
[4]*INRS Energie, Matériaux et Télécommunications, Université du Québec, Varennes (QC), Canada*
[5]*Department of Physics, University of Trieste, Trieste, Italy*
(Received 14 January 2005; revised manuscript received 8 April 2005; published 5 July 2005)

At a coverage of 5/3 monolayer (ML), Pb adsorbed on Ge(001) forms a ground phase displaying a $\binom{2\ 1}{0\ 6}$ symmetry. This phase undergoes two reversible phase transitions $\binom{2\ 1}{0\ 6} \leftrightarrow \binom{2\ 1}{0\ 3} \leftrightarrow (2\times 1)$ at the critical temperatures $T_{c_1} \sim 178$ K and $T_{c_2} \sim 375$ K, respectively. We investigated the behavior of the relevant order parameters at the critical temperatures by means of He and in-plane x-ray diffraction (HAS and XRD, respectively). Both phase transitions at the critical temperature put in evidence a clear order-disorder behavior, in agreement with the universality class expected for the corresponding symmetry group transformation. The low-temperature transition yields the critical exponent of the two-dimensional (2-D) Ising universality class, whereas the three-state Potts' critical exponents are found for the high-temperature transition. By out-of-plane XRD measurements, the low-temperature phase transition is observed to be accompanied by a static surface distortion at room temperature. A complementary HAS study of the temperature evolution of the surface charge corrugation reveals that the complete $\binom{2\ 1}{0\ 6} \leftrightarrow \binom{2\ 1}{0\ 3}$ transition is of the displacive type. On the contrary, the high-temperature phase transition does not show any change of the surface corrugation up to its irreversible decomposition, thus pointing to a pure order-disorder character.

DOI: 10.1103/PhysRevB.72.045404 PACS number(s): 68.35.Rh, 68.49.Bc, 61.10.Nz, 68.47.Fg

I. INTRODUCTION

The reconstructed semiconductor surfaces easily undergo surface phase transitions because the large energy excess produced by cutting a covalent crystal is only partially released by rehybridization of the dangling bonds. The most common, i.e., less energetically expensive, transitions are the order-disorder ones, which are triggered by dynamical fluctuations of the atomic structure, separating domains of antiphase order. Each domain is always in a ground structural configuration and the energetically expensive change of hybridization is confined to the domain boundary. When the domain size is reduced to a single lattice unit by the proliferation of domain walls, the interaction among structural fluctuations increases and a correlation can set in, possibly yielding a new stationary configuration of the surface electronic structure. In this case the transition is of the displacive type, the order-disorder behavior being simply an intermediate stage.[1] When the transition is driven by the electrons at the Fermi level, the corresponding charge redistribution takes the name of a charge density wave, CDW. In this case, atom displacement eventually occurs due to the recalling force exerted by the CDW on the ionic cores.

The possibility to induce charge density waves at metal/semiconductor interfaces well below their melting point is a subject of study in order to control the electronic properties at the interfaces of layered systems.[2] A viable route to this goal may be achieved through surface charge injection by submonolayer metal deposition. The most studied systems are certainly the 1/3 ML phases of metals on the (111) surfaces of Si and Ge, which can display phase transitions close to room temperature (RT).[3,4] Since the first claims of a surface charge density wave at the 1/3 ML Pb/Ge(111) surface,[3] many studies have shown that a sharp classification of the nature of these phase transitions is a difficult task. As an example, the well-known $(3\times 3) \leftrightarrow (\sqrt{3}\times\sqrt{3})$R30° transition at Sn/Ge(111) is now accepted to display a clear order-disorder character at the critical temperature of ~220 K due to dynamical fluctuations of the atomic structure,[5–7] but its behavior at a higher temperature is less clear. In fact, while a soft phonon has been observed at RT and attributed to the onset of a collective motion of the structural fluctuations,[8] the system still preserves its ground electronic configuration and local structure up to its irreversible decomposition at ~600 K.[9] In addition, the thermodynamical behavior is smeared by the perturbation of the surface charge density due to point defects and their reciprocal interaction.[10–12] Things are getting even more complicated when the Si(111) substrate is considered.[13–15] As a matter of fact, a comprehensive description of the 1/3 ML phase of metals on both Ge(111) and Si(111) is still a matter of discussion.

This family of submonolayer metal on semiconductor phases, while displaying a distinct metallicity at room temperature,[16,17] is characterized by a covalent bonding of the metal atoms to the substrate.[18] Moreover, the systems with the lower degree of metallicity, like the Sn/Si(111) one,[16] do not undergo any phase transition at all.[13] One might argue that a weaker bonding of the metal atoms to the substrate would probably be needed to allow the interface to undergo a neat displacive thermodynamical behavior. Such a configuration can be effectively obtained on the Ge(001) surface by deposition of 5/3 ML of Pb (where the coverage is expressed in terms of substrate atom density). This phase was already observed by both scanning probes (STM) and diffraction techniques (low-energy electron diffraction,

LEED, and XRD) to correspond to an almost metallic overlayer of Pb with a lateral atom density very close to that of a bulk Pb(111) plane.[19,20] This quasihexagonal Pb overlayer is slightly distorted by the substrate corrugation, thus yielding a commensurate lattice, whose structure was determined by an extended XRD study.[21] In particular, Bunk and co-workers found that the 5/3 ML low-temperature, LT phase displays a $\begin{pmatrix} 2 & 1 \\ 0 & 6 \end{pmatrix}$ ground symmetry, which transforms into a $\begin{pmatrix} 2 & 1 \\ 0 & 3 \end{pmatrix}$, at RT. From an analysis of the atomic anisotropic displacement parameters (which take into account both static and dynamical disorder), the transition was claimed to be driven by the height fluctuations of two particular Pb atoms in the $\begin{pmatrix} 2 & 1 \\ 0 & 6 \end{pmatrix}$ unit cell, as a consequence it was assigned to the order-disorder type.

In the present study, we focus on the characterization of the phase transition by studying the temperature dependence of the relevant order parameters. In addition, by performing detailed out-of-plane XRD measurements of a reference diffraction peak that is not involved in the transitions, we have determined whether its intensity variations are to be ascribed either to static or dynamic distortion of the Pb lattice. The resulting displacive character is found to be in agreement with the observed change of HAS diffracted intensity, reflecting a change of the surface charge corrugation. Finally, we have characterized also the $\begin{pmatrix} 2 & 1 \\ 0 & 3 \end{pmatrix} \leftrightarrow (2\times 1)$ reversible transition at $T_{c_2} \sim 375$ K.

II. EXPERIMENTAL

XRD measurements have been performed at the ALOISA beamline installed at the Elettra Synchrotron (Trieste, Italy). Both in-plane and out-of-plane (rod scans) diffraction data have been taken by keeping the surface at the critical angle. The rod scans were measured with a photon energy of 7000 eV, whereas a 6500 eV photon energy was used for azimuthal scans of the in-plane XRD peaks in a fixed $\theta - 2\theta$ scattering geometry. The He diffraction measurements have been performed with a HAS apparatus,[22] which is currently attached to the branch line of ALOISA. The HAS apparatus has a fixed scattering geometry ($\theta_{in} + \theta_{out} = 110$ deg) and the sample is mounted on a six-degrees-of-freedom manipulator for measuring the diffraction patterns. Most of the He diffraction patterns have been measured in continuous beam acquisition, while time-of-flight, TOF, acquisition has been used in a few cases to filter out the inelastic scattering contributions. Real time HAS measurements during deposition have been used for a fine tuning of the Pb optimal coverage (reproducibility of ~1% ML) and substrate growth temperature. The same recipe has been also adopted in the ALOISA end station by employing a reflection high energy electron diffraction (RHEED) system and specular x-ray reflectivity (XRR) for real time monitoring of Pb deposition. Both ALOISA and HAS make use of the same type of manipulator, thus allowing the exchange of sample holders (hosting thermocouples and heating filaments) for a better reproducibility of the preparation conditions.

The reciprocal lattice of the 5/3 ML phase is shown in Fig. 1. Due to the nonsquare symmetry of the unit cell, fractional spots at the 12th order appear along the main substrate

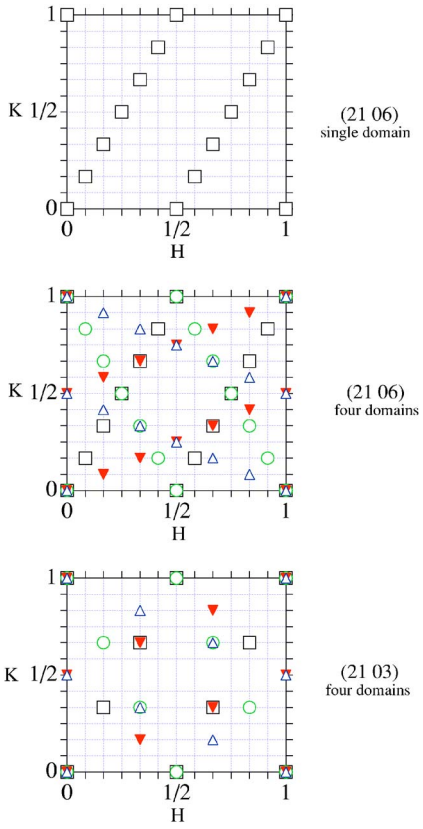

FIG. 1. (Color online) Upper panel: the unit cell of the $\begin{pmatrix} 2 & 1 \\ 0 & 6 \end{pmatrix}$ phase in the reciprocal space. The open squares represent the surface diffraction peaks of a single domain. Central panel: the $\begin{pmatrix} 2 & 1 \\ 0 & 6 \end{pmatrix}$ phase has a fourfold degeneracy due to the presence of four 90° rotated domains, shown with four different markers. Lower panel: the $\begin{pmatrix} 2 & 1 \\ 0 & 3 \end{pmatrix}$ phase is characterized by the disappearance of one peak every two along the [120] surface direction.

direction for the $\begin{pmatrix} 2 & 1 \\ 0 & 6 \end{pmatrix}$ ground phase [sixth-order spots for the $\begin{pmatrix} 2 & 1 \\ 0 & 3 \end{pmatrix}$ RT phase, from which it was also termed the "(2×6)" phase[20]]. Four equivalent domains are possible on the square substrate lattice, each one rotated by 90 deg (see the lattice construction from the first to the second panel in Fig. 1).

To single out the best preparation procedure (the one yielding the largest domains), we have monitored in real time the evolution of several HAS diffraction peaks during Pb deposition. In fact, several ordered structures are formed at RT by Pb on Ge(001) in the monolayer range, up to an incommensurate $c(4\times 8)-i$ phase at the saturation coverage of the first Pb layer, which is slightly larger than the 5/3 ML phase. At higher coverage, clusters are formed, which are in kinetic equilibrium with the $c(4\times 8)-i$ phase, and layer-by-layer growth can be only achieved at substrate temperature lower than 140 K.[23] The He diffracted intensity for a few peaks is shown in the upper panel of Fig. 2 for Pb deposition at RT. The optimal coverage for the 5/3 ML phase is witnessed by the maximum intensity of the (1/2,0) and (1/3,1/3) peaks. The appearance of the (1/4,0) peak, characteristic of the $c(4\times 8)-i$ phase, is clearly seen at slightly higher coverage. Thus, we have used the (1/3,1/3) peak (which is absent for all the other Pb/Ge phases of whatever

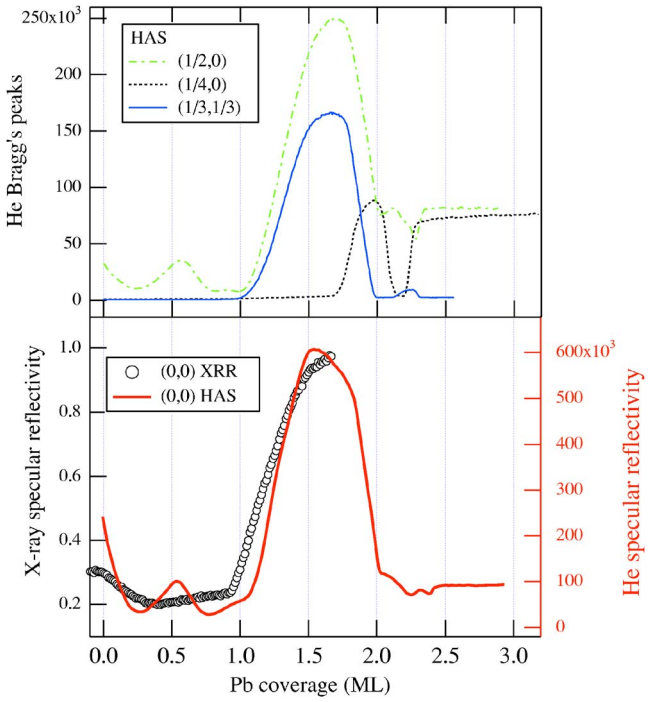

FIG. 2. (Color online) Upper panel: HAS intensity taken during Pb deposition at $T_s \sim 300$ K for a few off-specular diffracted peaks. The coverage is expressed in terms of substrate surface atom density. The absolute Pb coverage has been calibrated *a posteriori* on the maximum of the $(1/3,1/3)$ peak. The appearance of the $c(4\times 8)-i$ phase (first layer saturation coverage) is witnessed by the maximum of the $(1/4,0)$ peak. Lower panel: the specularly reflected x-ray and He intensity are reported on the left and right y axis, respectively. The XRR reflectivity coverage has been calibrated from LT layer-by-layer growth oscillations, according to Ref. 23.

coverage) as the reference peak for surface preparation. In the ALOISA preparation chamber, the correct coverage for the $\binom{2\ 1}{0\ 6}$ phase was found, from a comparison with RHEED patterns, to correspond to the first XRR intensity maximum (as shown in the lower panel of Fig. 2 together with the He specular reflectivity).

Each deposition was followed by a short flash to 400 K for annealing point defects. This procedure yielded the best diffraction peaks for the LT $\binom{2\ 1}{0\ 6}$ phase (in terms of both peak width and intensity), displaying reversible phase transitions with no appreciable hysteresis, as can be seen in Fig. 3 for the $\binom{2\ 1}{0\ 3} \rightarrow (2\times 1)$ phase transition. Annealing at a temperature higher than 450 K has been observed to reduce the surface quality. The last check of the surface quality was obtained *a posteriori* by measuring the transition temperature, since the best surface yields the highest critical temperature T_c.[24] Variations of T_c within ±5 K have been routinely obtained with our preparation procedure. Finally, the irreversible decomposition of the 5/3 ML Pb phase into a (1×5) is observed at about 550 K, in agreement with previous reports.[19,20]

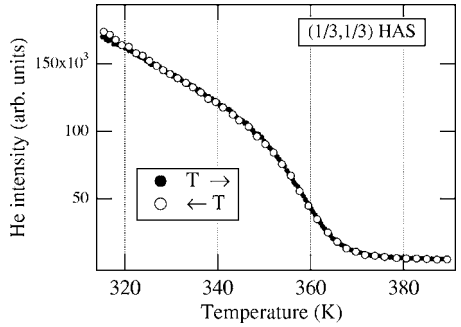

FIG. 3. The $(1/3,1/3)$ peak intensity is shown across the $\binom{2\ 1}{0\ 6} \rightarrow (2\times 1)$ transition. Filled and open markers show the phase transition measured with increasing and decreasing temperature, respectively, and evidence the absence of any detectable hysteresis. The sample has been kept only a few minutes at 400 K, before decreasing the temperature.

III. RESULTS AND DISCUSSION

A. Surface symmetries

The temperature dependence of a few diffracted peaks measured by HAS is shown in Fig. 4, which gives an overview of the phase transitions occurring at the 5/3 ML phase. The specularly reflected, integer, and half-integer peaks mainly display an intensity decrease due to Debye-Waller attenuation. The observed small deviations of these peaks from a regular exponential law will be discussed later, while here we focus on the $(5/12,1/6)$ and $(1/3,1/3)$ peaks [characterizing the $\binom{2\ 1}{0\ 6}$ and $\binom{2\ 1}{0\ 3}$ symmetries, respectively], which disappear, exhibiting a critical behavior (continuous and reversible intensity decrease accompanied by peak broadening) at two different temperatures (the inflection points being different by ~200 K).

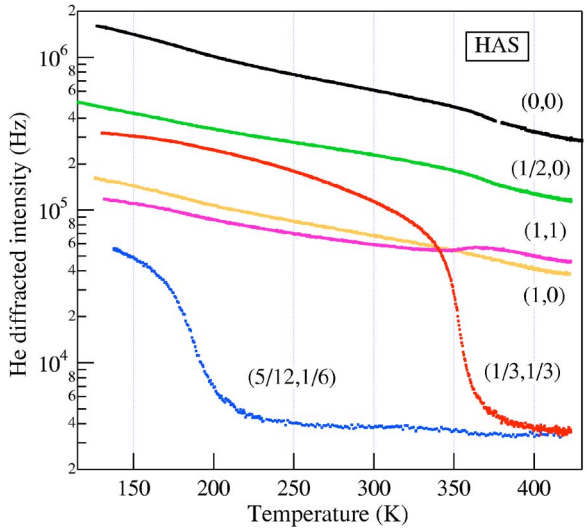

FIG. 4. (Color online) Temperature behavior of the He-diffracted peaks. The peak intensity is reported on a logarithmic scale to put in evidence the deviation from the Debye-Waller attenuation of the $(5/12,1/6)$ and $(1/3,1/3)$ peaks, due to the phase transitions. The specularly reflected (0,0) peak has been measured with the [100] surface direction aligned in the scattering plane.

At 400 K, the surface yields a (2×1) diffraction pattern, which is the highest symmetry observed on the 5/3 ML phase and probably reflects the Ge dimer reconstruction of the substrate underneath. In fact, Bunk and co-workers described the $\binom{2\ 1}{0\ 6}$ phase as a Pb layer on top of a $c(4\times2)$ dimer reconstructed substrate. The $\binom{2\ 1}{0\ 6}$ phase thus results by the occupation of one out of the six equivalent Ge(001) sublattices that are obtained shifting the $\binom{2\ 1}{0\ 6}$ lattice cell by a vector $(0,na)$, where a is the substrate surface unit cell and $n=0,1,\ldots,5$. The energy cost of creating a defect corresponding to a cell shift by na depends on the atomic structure of the Pb lattice cell, i.e., it is a function of n. The temperature hierarchy of the two observed phase transitions indicates that the $n=3$ defect type is the less expensive one. By thermal excitation of $n=3$-type defects, domain boundaries between regions of opposite $\binom{2\ 1}{0\ 6}$ order parameter are formed, which drive the system through a continuous phase transition into a $\binom{2\ 1}{0\ 3}$ high symmetry phase. According to the Landau's symmetry rules, such a two-spin system should display the critical behavior of a 2D-Ising universality class.

At a higher temperature the more expensive type of defects $n=1,2$ also starts to proliferate, reducing the $\binom{2\ 1}{0\ 3}$ long-range order. By symmetry arguments, we can neglect the underlying $\binom{2\ 1}{0\ 6}$ structure hidden in the RT phase, and, provided that these defects have the same energy cost, the $\binom{2\ 1}{0\ 3}$ phase can be mapped onto a three-spin system. Another order-disorder phase transition can thus take place, which should follow the three-state Potts' critical behavior at the critical temperature T_{c_2}.

B. Critical behavior

In order to check the hypothesis of two second-order phase transitions of the order-disorder (OD) type, we have studied the temperature behavior of the relevant long-range order parameters by means of surface diffraction. According to the reciprocal lattice shown in Fig. 1, the low symmetry vectors $\mathbf{G_i}$ of the 3rd, 6th, and 12th fractional order are characteristic of the surface symmetry in the LT and RT phases. In case of a second-order phase transition, the diffraction intensity for parallel momentum exchange $\mathbf{K}$ close to $\mathbf{G_i}$ can be approximated by[25]

$$I(\mathbf{K},T)=\rho^2(T)\,\delta(\mathbf{K}-\mathbf{G_i})+\chi(\mathbf{K}-\mathbf{G_i},T), \qquad (1)$$

where ρ stands for the order parameter, which only depends on the temperature, and χ represents the susceptibility accounting for the order fluctuations. In proximity of the critical temperature T_c, all the thermodynamical quantities scale as a power law of the reduced temperature $t=(T_c-T)/T_c$. The order parameter vanishes at T_c as $\rho\sim t^{\beta}$ and the susceptibility diverges as $\chi\sim|t|^{-\gamma}$. The Fourier transfrom of the susceptibility, which dominates the diffraction peak close to T_c, has a Lorentzian line shape, i.e., the peak width is inversely proportional to the fluctuations correlation length ξ, which also diverges at T_c as $\xi\sim|t|^{-\nu}$. For an equilibrium phase transition of the OD type, the critical exponents β,ν,γ are univocally determined by the surface symmetry. In particular, $\beta=1/8$, $\nu=1$, and $\gamma=7/4$ are predicted for the 2-D Ising model and $\beta=1/9$, $\nu=5/6$, and $\gamma=13/9$ for the three-state Potts' one.[26]

From an experimental point of view, the determination of the critical exponents from the study of the diffraction peaks is often hindered because of the smearing of the phase transitions at T_c due to finite size effects[27–29] and point defects,[30,31] so that power law behaviors are hardly observed for more than one decade in the logarithm of the reduced temperature. Moreover, an accurate analysis of the order parameter intensity behavior is complicated by the concurrent attenuation due to the Debye-Waller thermal fluctuations. In the case of HAS measurements, the diffracted intensity is also strongly affected by the occurrence of point defects (such as vacancies or impurities), since they have a very large cross section for thermal energy He atoms.[32] On the contrary, the width of the diffracted peaks (inversely proportional to the corresponding domain size) is unaffected by randomly distributed point defects. As a consequence, the determination of the critical temperature from the analysis of the fluctuation correlation length (exponent ν) is the most reliable one with diffractive techniques.

For HAS diffraction, the Lorentzian contribution to the peak broadening due to the order parameter fluctuations is convoluted with the instrumental peak profile (which is assumed to be Gaussian). Thus, the angular profiles taken at each temperature have been fitted to a Voigt function, where we have kept the width of the Gaussian component fixed to the value obtained by a fully free fit to the peak measured at the lowest achieved temperature. The resulting width of the Lorentzian component has been fitted to a power law for extracting the critical exponent. In the figures, we have also subtracted the value of the Lorentzian width obtained at the lowest temperature (which simply reflects the preexisting domain size distribution in the ground phase) to better highlight the broadening due to the domain wall proliferation. The temperature behavior of the $(1/2,1/4)$ HAS diffracted peak, characteristic of the LT $\binom{2\ 1}{0\ 6}$ phase, is shown in Fig. 5. From a comparison with similar diffraction experiments on other surfaces, it is worth noting the low degree of the rounding effect at T_{c_1}, which is indicative of a very good surface quality with low defect density. In fact, the peak broadening starts at a temperature where the intensity (i.e., the order parameter) is strongly reduced, unambiguously indicating the occurrence of an OD phase transition. The resulting critical exponent has been determined with good accuracy to be $\nu=1.04\pm0.08$ and the critical temperature $T_{c_1}=179\pm2$ K, confirming the assignment of the $\binom{2\ 1}{0\ 6}\leftrightarrow\binom{2\ 1}{0\ 3}$ phase transition to the 2D Ising universality class.

It should be remarked that the $(1/2,1/4)$ diffraction peak stems from the contribution of two kinds of equivalent surface domains, rotated by 180°, as can be seen from the central panel in Fig. 1. The OD critical exponents are not expected to be affected by this overlap, since they are independent from the direction along which the diffraction peak is collected.[33] As a check, we have also analyzed the $(5/12,1/6)$ HAS peak (shown in Fig. 6) which is originated by a single domain (see the central panel in Fig. 1). In this case, we have found a strong inelastic contribution (phonons) to the tails of the peak profile. As a consequence, we have

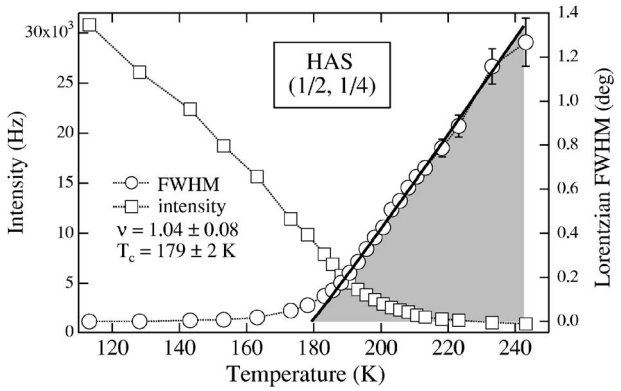

FIG. 5. Temperature dependence of the $(1/2,1/4)$ He diffraction peak taken along the [210] surface direction. The surface temperature during the acquisition of each point was kept constant within 0.2 K. The peak intensity (open squares, left y axis) and the Lorentzian FWHM (open circles, right y axis) were obtained by fitting the data to a Voigt function with a fixed Gaussian width of 0.1° due to the instrumental peak broadening. A Lorentzian width of 0.18°, as obtained for the lowest temperature, has been subtracted to better highlight the broadening due to the proliferation of domain walls. The full and shaded line is a fit to the Lorentzian width with the power law, as described in the text.

acquired its line shape in the TOF detection mode in order to retain the mere elastic contribution to He scattering. This choice has the drawback of a strong intensity decrease of the He beam, due to the low transmittance (0.5%) allowed by the chopper for TOF detection. Notwithstanding worse statistics, the so-obtained critical temperature $T_{c_1}=174\pm5$ K and critical exponent $\nu=0.99\pm0.27$ yield almost no discrepancy with respect to the $(1/2,1/4)$ peak.

The same analysis has been applied to the diffraction peaks involved in the high-temperature (HT) phase transition $\binom{2\ 1}{0\ 3}\leftrightarrow(2\times1)$. The intensity and width of the $(1/3,1/3)$ peak, as measured by HAS, is shown in Fig. 7. The smearing of this OD phase transition is further reduced with respect to the LT one. We found a critical exponent $\nu=0.84\pm0.11$ at a critical temperature $T_{c_2}=375\pm2$ K, confirming the three-state Potts' model. To check the homogeneity of this critical

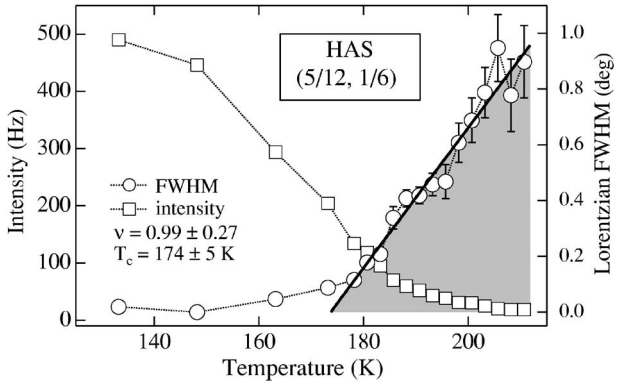

FIG. 6. Temperature dependence of the $(5/12,1/6)$ He diffraction peak taken along the [520] surface direction. A constant Gaussian width of 0.13° was used in the Voigt fit. The Lorentzian width at the lowest temperature was 0.12°. The same notation as in Fig. 5.

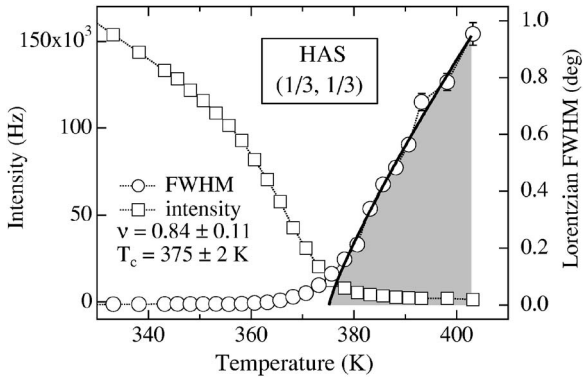

FIG. 7. Temperature dependence of the $(1/3,1/3)$ He diffraction peak taken along the [110] surface direction. A Gaussian width of 0.17° was used in the Voigt fit. The Lorentzian width at the lowest temperature was 0.09°. The same notation as in Fig. 5.

exponent, we have also studied the temperature behavior of the $(4/3,1/3)$ peak. For this peak, we show in Fig. 8 the intensity and width as measured by in-plane XRD. While the HAS angular profiles were taken by radial scans of the diffracted peaks, azimuthal scans have been collected for x-ray diffraction (XRD) measurements. For each temperature we have taken an azimuthal scan of the sample while keeping fixed the photon energy and the scattering geometry. In this way no instrumental broadening of the diffraction peak may take place and the angular profile of the diffraction peak is always found to be a pure Lorentzian. Fitting the width to a power law yields $\nu=0.84\pm0.03$ at $T_{c_2}=362\pm1$ K, in excellent agreement with the predicted $\nu=5/6$ value.[34] It is worth noting that in this case the power law behavior is found to extend for more than one decade of the peak width (see the right y axis of Fig. 8).

Both phase transitions, at the corresponding critical temperature, display a very neat order-disorder character. In particular, it is very tempting to associate the $\binom{2\ 1}{0\ 6}\leftrightarrow\binom{2\ 1}{0\ 3}$ transition with the $c(4\times2)\leftrightarrow(2\times1)$ of the clean Ge(001) surface. The latter also belongs to the 2D Ising class and was

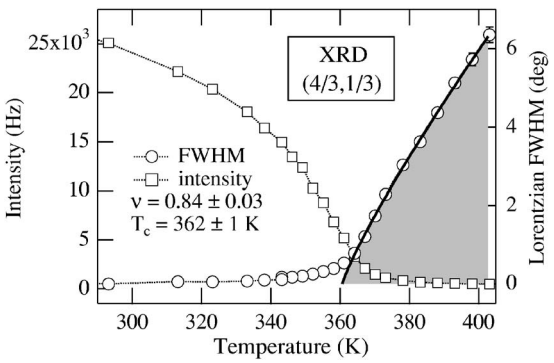

FIG. 8. Temperature dependence of the $(4/3,1/3)$ peak taken by in-plane XRD. Azimuthal scans have been performed with a 6500 eV photon energy, while keeping the sample at the critical angle of 0.4°. The peak intensity and the Lorentzian FWHM were obtained by fitting the data to a pure Lorentzian function. The Lorentzian width at the lowest temperature was 0.197°. The same notation as in Fig. 5.

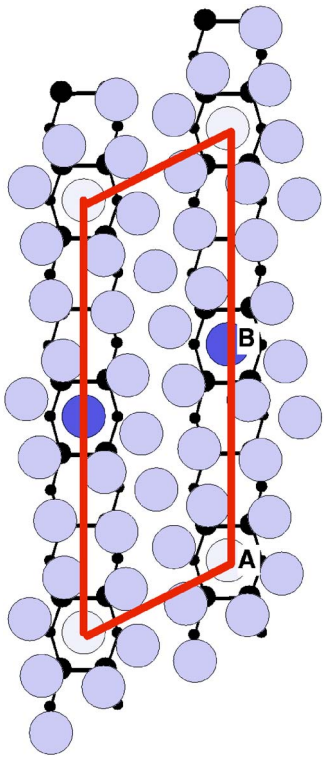

FIG. 9. (Color online) Top view of the structural model proposed in Ref. 21 for the $\binom{2\ 1}{0\ 6}$ phase. Pb atoms are represented by the large grey circles, the underlying Ge atoms are represented by the small filled circles, and the surface unit cell is also drawn (the lozenge with thick lines). The brighter and darker circles (labeled *A* and *B*, respectively) are the only Pb atoms in high symmetry sites and, according to Bunk and co-workers, their vertical height differs by ~1.5 Å.

reported to occur at a critical temperature of 240 K,[35] where the Ge dimers can flip the orientation of their buckling angle, i.e., losing the ground phase correlation, where adjacent dimers order with opposite buckling orientation.[36,37] According to the structural model by Bunk and co-workers, the Pb overlayer can be regarded as a sheet of Pb atoms standing at a large mean height above the weakly interacting dimer reconstructed substrate, as depicted in Fig. 9. In fact, only two Pb atoms per unit cell (labeled *A* and *B* in Fig. 9) are found in correspondence of a substrate high symmetry site (the pedestal site, coordinated to four Ge atoms), thus suggesting a stronger (possibly covalent) interaction.[21] In this case, the manifestation of a $n=3$ type of defect (antiphase domain wall for the $\binom{2\ 1}{0\ 6}$ phase) might be triggered by the flipping of the substrate dimers, which only affect the Pb atoms interacting more strongly with Ge atoms. The lower critical temperature for the 5/3 ML Pb/Ge system can be simply attributed to the larger instability of the dimer correlation in the $c(4\times2)$ phase, when covered by the Pb sheet. Still, this model, drawn on the basis of the long-range order parameter analysis, does not exclude the occurrence of a late stage displacive character due to the onset of a collective motion of the fluctuations.

C. Displacive character

The $\binom{2\ 1}{0\ 3}$ phase is best suited to pursue an investigation in search of static distortions, since it is well confined between the lower and upper limits of the two critical temperatures. In their XRD study, Bunk and co-workers already found a change of the intensity for a few rod scans taken on XRD peaks that are present in both the LT and RT phases.[21] From their fittings, these changes were attributed to an increase (from LT to RT) of the vertical anisotropic displacement parameter, ADP, associated with the Pb atoms at the apex of the $\binom{2\ 1}{0\ 3}$ unit cell (labeled *A* and *B* in Fig. 9). As a consequence, the two Pb atoms *A* and *B*, simply differing by their vertical height in the ground phase at low temperature, can flip between the up and down positions, thus originating a defect of the $n=3$ type in the $\binom{2\ 1}{0\ 6}$ surface lattice.

The ADP adopted by Bunk and co-workers is an effective parameter accounting for both static and dynamical disorder at the corresponding coordination site, thus it is not well suited to detect the onset of a displacive character in the Pb height fluctuations. The set of experimental data and fitting parameters presented by Bunk was already so large that a refinement of the structural investigation does not seem a viable route to achieve the discrimination between the static and dynamical models. We followed a different approach by restricting our XRD study to the detailed comparison of a few XRD rod scans, not involved in the transitions, as taken at different temperatures. The rod scans probe the vertical structure of the substrate and any deviation from a regular bulk-truncated atom periodicity gives rise to an *L* modulation of the rod. Disorder, either static or dynamic, does not change the average position of the atoms and only produces a diffracted intensity decrease. On the contrary, a change of the rod scan modulation is expected when the atom fluctuations driving the OD transition are accompanied by a displacement of the equilibrium atom positions. The direct comparison between rod scans taken at two different temperatures is not straightforward because of the Debye-Waller attenuation along the rod ($\propto e^{-DW\cdot T\cdot L^2}$), strongly smearing the data at large *L* values.

The $(3/2,2,L)$ rod is well suited for a detailed XRD study since it displays a well defined feature at large *L* values, where the sensitivity to a vertical distortion is higher. In the upper panel of Fig. 10, the integrated intensity along the rods is reported for three temperatures 173 (LT), 273 (RT), and 373 K (HT), representative of the $\binom{2\ 1}{0\ 6}$, $\binom{2\ 1}{0\ 3}$ and (2×1) phases, respectively. The LT rod scan displays a different *L* dependence with respect to the RT and HT ones. The latter two mainly differs at large *L* values, i.e., where a stronger DW attenuation factor dominates. For a better comparison, the rod scans have been divided by an effective exponential attenuation. The latter was obtained from the ratio between the RT and HT rod scans in the limited range $4\leqslant L^2\leqslant 9$. In fact, the $(3/2,2,L)$ rod is almost unchanged in the $\binom{2\ 1}{0\ 3}$ and (2×1) phases; thus the logarithm of the ratio has a smooth linear dependence on L^2, whose slope yields $DW=0.7\times10^{-3}$. We have divided for this attenuation the LT rod scan as well. In fact, the *DW* coefficient is not expected to change dramatically for the LT phase transition (as can be seen from the smooth behavior of all the He-diffracted peaks shown in Fig. 4), and the strong attenuation of the rod scan with *L* can be effectively taken into account.

As can be seen in the lower panel of Fig. 10, the rod scans taken at LT and RT display a large difference for $L\leqslant0.5$, a

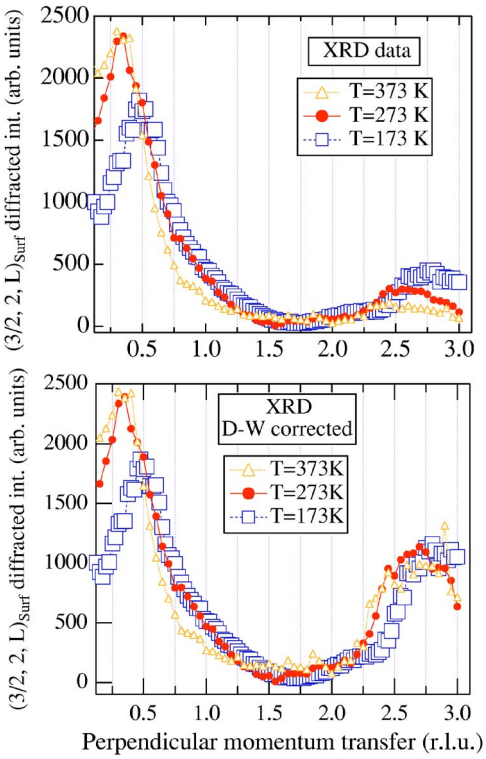

FIG. 10. (Color online) The XRD $(3/2,2,L)$ rod scans are shown for three surface temperatures: 173 K open squares, 273 K filled circles, and 373 K open triangles. Upper panel: the integrated intensity along the rod is shown after simple correction for the ALOISA scattering geometry. Lower panel: the same rod scans are shown after correction for the Debye-Waller attenuation (see the text).

significant shift ($\Delta L \sim -0.2$) of the feature at $L \sim 2.7$ and the disappearance of the LT shoulder at $L \sim 2.2$. On the contrary, the RT and HT rod scans, taken with the same temperature increase $\Delta T = 100$ K, are very similar and the only difference is a narrowing of the main feature at $L \sim 0.3$. We remark that the observed variations of the $(3/2,2,L)$ rod are not simply related to the intensity, but rather to the position and shape of the rod features, i.e., they indicate the occurrence of a vertical structural distortion in the $\binom{2\ 1}{0\ 3}$ phase, which is also preserved in the (2×1) phase.

The $(3/2,2,L)$ rod scans, while sufficient to assign a displacive character to the $\binom{2\ 1}{0\ 6} \leftrightarrow \binom{2\ 1}{0\ 3}$ phase transition, yield little information about the second transition. Even if the rod scan does not change between RT and HT, the transition might still be a displacive one, whose observation failed either because the temperature for the rod scan was not high enough, or because the eventual structural distortion does not yield any contribution to the present rod. To better address this issue, we have obtained complementary information about the change of the surface charge corrugation by the analysis of the temperature variation of the off-specular HAS diffraction.

Due to its extreme surface sensitivity, HAS is well suited to detect a redistribution of surface charge density, be it with or without any accompanying structural distortion. From this point of view, the envelope of the HAS-diffracted peaks

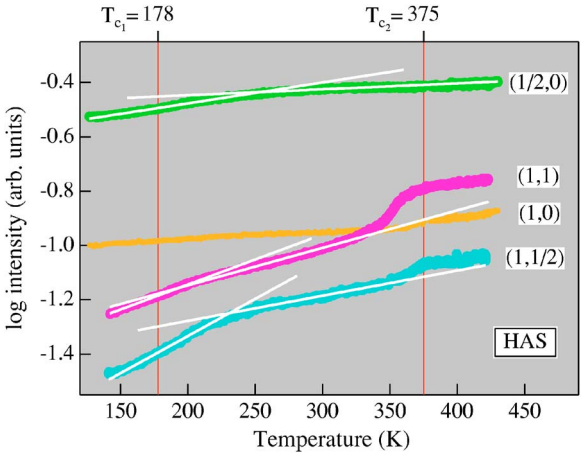

FIG. 11. (Color online) The temperature dependence of the HAS diffraction peaks is shown after normalization to the specular (0,0) peak, as taken with the same azimuthal orientation of the corresponding diffraction peak. As a guide to the eye, the linear fits to the logarithm of the relative intensity are superimposed to the data to highlight the change of slope.

maps the surface charge corrugation in the reciprocal space like STM topography does in the direct space. A remarkable difference between the two techniques is the very short interaction time of HAS ($\sim 10^{-10}$ s) with respect to STM ($\sim 10^{-6}$ s), which is relevant in the present case to discriminate between static and dynamical distortions. In a semiclassical approach, the He-surface potential can be approximated by a corrugated hard wall (i.e., the attractive part of the potential is neglected, as well as the occurrence of a potential well), then the He-diffracted intensity simply reflects the unit cell form factor.[32] Any change of the surface charge corrugation should appear as a change in the relative peak intensity. The relative intensity of the high symmetry peaks, common to the LT, RT, and HT phases, is shown in Fig. 11. By visual inspection, each peak in the logarithmic scale displays a segmented behavior with temperature. For a given structure, this linear behavior is expected since each diffraction peak undergoes a slightly different Debye-Waller attenuation due to different vertical momentum transfer of the He beam.

We have fitted the linear segments of the logarithm of the peak intensity to straight lines, whose extrapolation puts in evidence the change of slope in passing from one phase to another. The LT $\binom{2\ 1}{0\ 6}$ and RT $\binom{2\ 1}{0\ 3}$ phases clearly display a change of the line slopes for all the peaks, but the (1, 0). The change of slope does not occur at the critical temperature ${}^{OD}T_{c_1} \sim 178$ K of the 2-D Ising transition, but some 50 K higher. The variation of the Debye-Waller attenuation is due to a change of the root mean square displacement of the surface atoms, hence the DW change of slope really marks a change of the surface charge corrugation. We remark that in the scattering geometry of our HAS apparatus, there is an enhanced coupling between the He beam and the vertical displacement of the surface atoms.[38] The observed variation of the surface charge corrugation can thus be consistently associated with the vertical distortion of the surface structure that has been put in evidence by the rod scan analysis.

The change of the corrugation at a temperature higher than the OD transition reflects the fact that the $\binom{2\ 1}{0\ 6}$ order

parameter correlation length has reached its minimum (compare with Fig. 5), where an interaction between antiphase boundaries ($n=3$-type defects) can set in, and structural displacement occurs.[1,39] The microscopic mechanism claimed to drive this transition (height fluctuations of two nonequivalent atoms in high symmetry sites[21]) closely resembles that of the $(3\times3)\leftrightarrow(\sqrt{3}\times\sqrt{3})R30°$ transition at 1/3 ML Sn/Ge(111).[6] In the latter case, the Sn height fluctuations were found to determine an OD critical behavior at $T_c \sim 220$ K,[5] and to evolve into a collective motion (phonon) at room temperature.[8] Still these fluctuations do not evolve into a static change of the surface bond hybridization, since the average height of the individual Sn atoms does not change up to the temperature of decomposition ($\sim$600 K) of the $(\sqrt{3}\times\sqrt{3})R30°$ phase.[8,9] The present system is exceptional in the manifestation of a displacive character below room temperature, since much higher temperatures are usually required to induce a static modification or breaking of the covalent bonds in semiconductor systems. For comparison, a change of surface corrugation on the clean Ge(001) surface was reported by HAS for the $(2\times1)\leftrightarrow(1\times1)$ transition at $\sim$950 K.[35]

The interpretation of the HAS peak intensity at the $\binom{2\ 1}{0\ 3}\leftrightarrow(2\times1)$ phase transition is not straightforward. A steplike increase of the relative intensity is observed for a few peaks just below the critical temperature ${}^{OD}T_{c_2}\sim375$ K, but the same linear slope of the RT phase is recovered to within $\sim$20 K. Since the RT Debye-Waller coefficient is recovered at the disappearance of the order parameter, we do not associate the increase of the relative peaks with a variation of the surface structure, but rather to a multiple scattering effect.

On a corrugated surface, such as the $\binom{2\ 1}{0\ 3}$ one, there are many diffraction channels that can be coupled with multiple scattering events at the repulsive potential wall and with multiple hopping in the potential well. When the $\binom{2\ 1}{0\ 3}\leftrightarrow(2\times1)$ phase transition takes place, most of these channels are turned off and the corresponding scattered intensity is redistributed among the remaining diffraction channels. The semiclassical approximation, where the relative peak intensity reflects the surface corrugation, breaks down and full quantum scattering calculations with a reliable He-surface interaction potential are required to correctly describe the He scattered intensity.[40] This kind of calculations is far from being settled for a complex system like the present one, however, our interpretation is consistent with the fact that the steplike increase of the relative intensity occurs at the disappearance of the order parameter and not at temperature higher than ${}^{OD}T_{c_1}$, as would be expected in case of a displacive phase transition. In fact, a similar increase of the peak intensity at the disappearance of the surface order parameter was already observed for a pure 2-D-Ising OD phase transition on a different system.[41]

The $\binom{2\ 1}{0\ 3}\leftrightarrow(2\times1)$ phase transition at 5/3 ML Pb/Ge(001) thus appears as an order-disorder one, even if we cannot exclude the manifestation of a structural distortion beyond 450 K, where our measurements are hindered by the degradation of the 5/3 ML Pb phase. Finally, the fact that the Debye-Waller attenuation is the same in the RT and HT phases confirms the validity of the procedure used to extract the *DW* coefficient from the rod scans.

IV. SUMMARY

Deposition of 5/3 ML of Pb on Ge(001) yields a $\binom{2\ 1}{0\ 6}$ ground phase that undergoes a reversible phase transition to a $\binom{2\ 1}{0\ 3}$ symmetry at $T_{c_1}\sim178$ K. A second reversible phase transition into a (2×1) symmetry is observed at $T_{c_2}\sim375$ K. From the study of the relevant order parameter correlation length, the two phase transitions are assigned to the order-disorder 2D Ising and three state Pott's universality class, respectively. In between the two critical temperatures, the 5/3 ML phase is also found to be affected by a distortion of its atomic structure and corrugation of the surface charge density, while preserving the $\binom{2\ 1}{0\ 3}$ symmetry. As a consequence, the $\binom{2\ 1}{0\ 6}\leftrightarrow\binom{2\ 1}{0\ 3}$ transition must be regarded as a displacive phase transition with an intermediate order-disorder stage.

ACKNOWLEDGMENT

We are grateful to Francesco Bruno for assistance in XRD simulations.

*Corresponding author. Fax: +39-040-226767. Electronic address: floreano@tasc.infm.it

[1] For a review on displacive phase transitions see, e.g., A. D. Bruce, and R. A. Cowley, Adv. Phys. **29**, 219 (1980).

[2] For an overview on surface CDW transitions see, e.g., E. Tosatti, in *Electronic Surface and Interface States on Metallic Systems*, edited by E. Bertel and M. Donath (World Scientific, Singapore, 1995).

[3] J. M. Carpinelli, H. H. Weitering, E. W. Plummer, and R. Stumpf, Nature (London) **381**, 398 (1996).

[4] J. M. Carpinelli, H. H. Weitering, M. Bartkowiak, R. Stumpf, and E. W. Plummer, Phys. Rev. Lett. **79**, 2859 (1997).

[5] L. Floreano, D. Cvetko, G. Bavdek, M. Benes, and A. Morgante, Phys. Rev. B **64**, 075405 (2001).

[6] J. Avila, A. Mascaraque, E. G. Michel, M. C. Asensio, G. Le Lay, J. Ortega, R. Pérez, and F. Flores, Phys. Rev. Lett. **82**, 442 (1999).

[7] R. I. G. Uhrberg, H. W. Zhang, and T. Balasubramanian, Phys. Rev. Lett. **85**, 1036 (2000).

[8] D. Farias, W. Kaminski, J. Lobo, J. Ortega, E. Hulpke, R. Perez, F. Flores and E. G. Michel, Phys. Rev. Lett. **91**, 016103 (2003).

[9] L. Petaccia, L. Floreano, A. Goldoni, D. Cvetko, A. Morgante, L. Grill, A. Verdini, G. Comelli, G. Paolucci, and S. Modesti, Phys. Rev. B **64**, 193410 (2001).

[10] H. H. Weitering, J. M. Carpinelli, A. V. Melechko, J. Zhang, M. Bartkowiak, and E. W. Plummer, Science **285**, 2107 (1999).

[11] A. V. Melechko, J. Braun, H. H. Weitering, and E. W. Plummer, Phys. Rev. Lett. **83**, 999 (1999).

[12] L. Petersen, Ismail, and E. W. Plummer, Prog. Surf. Sci. **71**, 1 (2002).

[13] H. Morikawa, I. Matsuda, and S. Hasegawa, Phys. Rev. B **65**, 201308(R) (2002).
[14] L. Ottaviano, B. Ressel, C. Di Teodoro, G. Profeta, S. Santucci, V. Cháb, and K. C. Prince, Phys. Rev. B **67**, 045401 (2003).
[15] A. A. Escuadro, D. M. Goodner, J. S. Okasinski, and M. J. Bedzyk, Phys. Rev. B **70**, 235416 (2004).
[16] B. Ressel, J. Slezak, K. C. Prince, and V. Cháb, Phys. Rev. B **66**, 035325 (2002); B. Ressel, C. Di Teodoro, G. Profeta, L. Ottaviano, V. Cháb, and K. C. Prince, Surf. Sci. **562**, 128 (2004).
[17] A. Goldoni and S. Modesti, Phys. Rev. Lett. **79**, 3266 (1997); **81**, 3553 (1998).
[18] S. De Gironcoli, S. Scandolo, G. Ballabio, G. Santoro, and E. Tosatti, Surf. Sci. **454–456**, 172 (2000).
[19] G. Falkenberg, L. Seehofer, R. Rettig, and R. L. Johnson, Surf. Sci. **372**, 155 (1997).
[20] Y. Zhang, R. G. Zhao, and W. S. Yang, Surf. Sci. Lett. **293**, L821 (1993).
[21] O. Bunk, M. M. Nielsen, J. H. Zeysing, G. Falkenberg, F. Berg-Rasmussen, M. Nielsen, C. Kumpf, Y. Su, R. Feidenhans'l, and R. L. Johnson, New J. Phys. **3**, 13 (2001).
[22] D. Cvetko, A. Lausi, A. Morgante, F. Tommasini, K. C. Prince, and M. Sastry, Meas. Sci. Technol. **3**, 997 (1992).
[23] L. Floreano, D. Cvetko, F. Bruno, G. Bavdek, A. Cossaro, R. Gotter, A. Verdini, and A. Morgante, Prog. Surf. Sci. **72**, 135 (2003).
[24] B. N. J. Persson, Surf. Sci. Rep. **15**, 1 (1992).
[25] R. F. Willis, in *Dynamical Phenomena at Surfaces, Interfaces and Superlattices 2*, edited by F. Nizzoli, K.-H. Rieder, and R. F. Willis (Springer-Verlag, Berlin, 1985), Vol. 11.
[26] M. Schick, Prog. Surf. Sci. **11**, 245 (1981).
[27] A. E. Ferdinand and M. E. Fisher, Phys. Rev. **185**, 832 (1969).
[28] D. P. Landau, Phys. Rev. B **13**, 2997 (1976).
[29] M. Sokolowski and H. Pfnür, Phys. Rev. B **49**, 7716 (1994).
[30] K. Inoue, Y. Morikawa, K. Terakura, and M. Nakayama, Phys. Rev. B **49**, R14774 (1994).
[31] Y. Nakamura, H. Kawai, and M. Nakayama, Phys. Rev. B **55**, 10549 (1997).
[32] D. Farias and K.-H. Rieder, Rep. Prog. Phys. **61**, 1575 (1998).
[33] D. Cvetko, V. De Renzi, L. Floreano, A. Morgante, and F. Tommasini, Solid State Commun. **91**, 539 (1994).
[34] The discrepancy between the critical temperatures obtained by HAS and XRD has been attributed to the different calibration of the electronics employed to read the thermocouple output voltage, while the same sample and sample holder have been used in the two experimental chambers.
[35] D. Cvetko, L. Floreano, A. Crottini, A. Morgante, and F. Tommasini, Surf. Sci. Lett. **447**, L147 (2000).
[36] S. D. Kevan, Phys. Rev. B **32**, 2344 (1985).
[37] S. Ferrer, X. Torrelles, V. H. Etgens, H. A. van der Vegt, and P. Fajardo, Phys. Rev. Lett. **75**, 1771 (1995).
[38] M. Buongiorno Nardelli, D. Cvetko, V. De Renzi, L. Floreano, A. Morgante, M. Peloi, and F. Tommasini, Phys. Rev. B **52**, 16720 (1995).
[39] H. J. Ernst, E. Hulpke, and J. P. Toennies, Phys. Rev. B **46**, 16081 (1992).
[40] D. Cvetko, V. De Renzi, L. Floreano, A. Lausi, A. Morgante, M. Peloi, F. Tommasini, E. Kirsten, and K.-H. Rieder, Phys. Rev. B **51**, 11055 (1995).
[41] A. F. Bellman, D. Cvetko, A. Morgante, M. Polli, F. Tommasini, K. C. Prince, and R. Rosei, Surf. Sci. Lett. **281**, L321 (1993).